De Assis, G. C., Skovroinski, E., Leite, V. D., Rodrigues, M. O., Galembeck, A., Alves, M. C. F., ... De Oliveira, R. J. (2018). Conversion of "Waste Plastic" into Photocatalytic Nanofoams for Environmental Remediation. *ACS Applied Materials and Interfaces*, *10*(9), 8077-8085. https://doi.org/10.1021/acsami.7b19834

Article

Conversion of "waste plastic" into photocatalytic nanofoams for environmental remediation

Geovânia Cordeiro de Assis, Euzébio Skovroinski, Valderi Duarte Leite, Marcelo Oliveira Rodrigues, André Galembeck, Mary Alves, Julian Eastoe, and Rodrigo Jose de Oliveira

ACS Appl. Mater. Interfaces, **Just Accepted Manuscript** • DOI: 10.1021/acsami.7b19834 • Publication Date (Web): 20 Feb 2018

Conversion of "Waste Plastic" into Photocatalytic Nanofoams for Environmental Remediation

Geovania C. de Assis [§Δ]*; Euzébio Skovroinski* [¥]*; Valderi D. Leite* [§]*; Marcelo O. Rodrigues* [†]*; André Galembeck* [¦]*; Mary C.F. Alves* [§]*; Julian Eastoe* [‡]**; Rodrigo J. de Oliveira* [§]***

[§] Departamento de Química, Universidade Estadual da Paraíba, 58429-500, Brazil.

[¥] Programa de Pós-Graduação em Ciência de Materiais, Universidade Federal de Pernambuco, 50740-540, Brazil.

[¦] Departamento de Química Fundamental, Universidade Federal de Pernambuco, 50740-540, and CETENE, MCTI, 50740-545, Brazil.

[†] Instituto de Química, Universidade de Brasília, 70297-400, Brazil.

[‡] School of Chemistry, University of Bristol, BS8 1TS, UK.

Abstract

Plastic debris is a major environmental concern, and to find effective ways to reuse polystyrene (PS) presents major challenges. Here it is demonstrated that polystyrene

foams impregnated with SnO_2 are easily generated from plastic debris, and can be applied to photocatalytic degradation of dyes. SnO_2 nanoparticles were synthesized by a polymeric precursor method, yielding specific surface areas of 15 m^2/g after heat treatment to 700 ºC. Crystallinity, size and shape of the SnO_2 particles were assessed by X-ray diffraction (XRD) and transmission electron microscopy (TEM), demonstrating the preparation of crystalline spherical nanoparticles with sizes around 20 nm. When incorporated into PS foams, which were generated using a thermally induced phase separation (TIPS) process, the specific surface area increased to 48 m^2/g. These PS/SnO_2 nanofoams showed very good efficiency for photodegradation of Rhodamine B, under UV irradiation, achieving up to 98.2% removal. In addition the PS/SnO_2 nanofoams are shown to retain photocatalytic activity for up to five reuse cycles.

Keywords: environmental remediation, nanocatalysis, dye degradation, porous catalyst, polymer waste, plastic reuse.

1. INTRODUCTION

A wide range of toxic and hazardous substances, including synthetic dyes, are continuously being released into wastewaters, mostly due to lack of effective treatment methods[1]. Dyes are used by various industries, however, recent studies have demonstrated that they are responsible for serious damage to aquatic ecological systems[2]. Rhodamine B (RhB) is a fluorone type organic dye belonging to the xanthene family, and studies suggest that RhB is carcinogenic, as well as a chronic reproductive and neuro toxin to humans and animals[3], and to a lesser extent an allergen[4]. Therefore development of methods for degradation of dyes like RhB in industrial effluents are of high importance[5].

Recently, numerous new approaches have been developed for removing pollutants from wastewater[6]. Advanced oxidation processes (AOP)[7] hold particular promise for degradation of organic contaminants. Among these AOP methods, heterogeneous photocatalysis is very attractive offering the potential to turn organic contaminants into mineral salts and end products such as CO_2 and H_2O[8–11]. Various metal oxides, such as, TiO_2, ZnO, ZnS, WO_3, CdS, SnO_2, among others, can be used as semiconductors for heterogeneous photocatalysis and degradation[12]. In addition, nanostructured materials have been widely studied owing to beneficial properties, such as high electrical conductivity, high transparency in the visible region, high thermal, mechanical and chemical stability, and for potential applications in optically transparent materials and liquid crystal displays[13], catalysts, gas sensors[14] and solar cells[15].

Catalytic nanoparticles, such as SnO_2, are generally supported on substrates to facilitate separation and reuse from the reaction medium[16]. A variety of catalyst support morphologies have been studied, including fibers, three dimensional networks and other complex shapes[17]. In this regard, foams appear to be very promising supports for photocatalysts, since they present different length scales from nano- to millimeter, facilitating dispersion and support of nanoparticles, whilst also providing large surface areas in mechanically robust 3-D network structures of macroscopic dimensions. A procedure for obtaining micro- and nano-structured polymeric foams was introduced by Aubert and Clough[18], by mixing polystyrene (PS) with a mixture of cyclohexane (CH)/benzene. Eastoe *et al*[19] also developed foams of surfactant-stabilized $CaCO_3$ nanoparticles using thermally induced phase separation (TIPS) from cyclohexane dispersions. Based on these previous reports it is of interest to see if semiconductor-containing foams can offer increased efficiency of organic pollutant photocatalytic degradation. Additionally, there is a need to find useful applications for waste

polystyrene. The aim of this article is to combine these two issues to explore reuse of PS for the development of PS/SnO_2 based nanofoams, and then to evaluate these photocatalytic systems for potential applications in environmental remediation of RhB by photo-degradation.

2. EXPERIMENTAL SECTION

2.1 Materials

Citric Acid ($C_6H_8O_7.H_2O$) (Cargill / 99.5% purity), Ethylene Glycol ($HO.CH_2.CH_2.OH$) (Avocado / 99.0% purity), nitric acid (HNO_3) (Dinâmica / 65.0% purity), tin chloride ($SnCl_2.2H_2O$) (Dinâmica / 98.0 to 103.0% purity), cyclohexane (CH, C_6H_{12}) (Sigma-Aldrich) and polystyrene (PS) obtained in the form of pellets sold in a local market, were used as received.

2.2 Synthesis of nanoparticles of SnO_2

The SnO_2 nanoparticles were synthesized by the polymeric precursor method[20]. Initially, 319.122 g of citric acid was dissolved in 1,000 mL of water and then, 125.000 g of tin chloride was added to the solution under stirring. The molar ratio of tin (II) chloride dihydrate to citric acid was 1:3. After complete dissolution, 22 mL of ammonium hydroxide aqueous solution was added to the mixture. The system was cooled in an ice/water mixture to facilitate the precipitation of tin citrate. After separation, 8.000 g of the tin citrate was dissolved at room temperature in 2.000 mL of H_2O and, to complete the dissolution, 8.000 mL of nitric acid were slowly added. Ethylene glycol was added to the previous solution, in a ratio of 40:60 with respect to the total amount of citric acid and then stirred at 70 °C to occur release of NOx gases, leading to a reduction in resin weight by about one half. Polymerization occurs through an esterification reaction between citrate and ethylene glycol, thereby obtaining a

polyester with homogeneously distributed metal ions. After the reaction, a polymer resin was formed and this resin was then placed in a muffle furnace EDG-01 at a temperature of 350°C for 2 hours under an air atmosphere, to partially remove organic matter. In this step, the polymer chains present in the resin were decomposed yielding a so called expanded resin precursor, being similar to a sponge material of dark coloration, which was removed from the furnace and powdered in a mortar. The powder precursor material was then treated at temperatures of 700, 800 and 900°C for 2 hours in an air atmosphere and named as SnO_2-700, SnO_2-800 and SnO_2-900.

2.3 Synthesis of SnO_2 impregnated polystyrene nanofoams (PS/SnO_2 nanofoams)

The PS/SnO_2 nanofoams were obtained by a TIPS process[21] combined with lyophilization[22]. The PS content in cyclohexane mixture ranged from 1.0, 2.5 to 5.0% (w/v) and the concentration of SnO_2 in the nanofoams was also varied (2.5 and 5.0%, w/w relative to PS mass). The samples were labeled as PS(X)/SnO_2(Y), where X is the percentage (w/v) of PS in CH and Y is the percentage (w/w) of SnO_2 relative to PS. PS/CH mixture was sonicated for 3 hours in an ultrasonic bath to complete polystyrene dissolution in the solvent. For example, to prepare the colloidal dispersion for PS(2.5)/SnO_2(5) nanofoams, 0.0625 g of SnO_2 was added to 5 ml of 2.5% PS solution, and then kept for 2 hours in an ultrasound bath, to allow the formation of the colloidal dispersion. The dispersions were frozen using a Peltier system, (Fig. S1 in Supporting Information) at -10 ° C (the freezing point of CH is + 6 ° C). After 10 minutes of cooling, a vacuum pump was connected to remove the CH solvent by lyophilization for 30 minutes. This technique results in the removal of the frozen CH solvent based on sublimation[23]. Tests were performed to find the optimal time for obtaining the foams. The low pressure freeze-drying led to cyclohexane removal by sublimation in the sample leaving behind a solid foam with a hard "skeleton".

2.4 Characterization

All samples were characterized by X-Ray Diffraction (XRD) analysis in a Miniflex diffractometer 300 of RIGAKU with Cu Ka radiation, 2 kVA power, voltage of 30 kV and current of 30 mA. Scans were made in the range of 2θ between 10 and 80 ° with a step of 0.02 ° and speed of $2°s^{-1}$. The B.E.T. surface area of the samples was estimated by N_2 adsorption analysis at 77 K in a surface area analyzer from Quanta Chrome Instruments, New Model 2200E. The samples were treated at 80 °C for 3 h under vacuum until reaching a pressure lower than 10 μm Hg. Transmission electron microscopy was conducted using a FEI Tecnai 20 instrument, with acceleration voltage of 200kV, at the Centro de Tecnologias Estratégicas do Nordeste - CETENE.

2.5 Evaluation of Photocatalytic Activity

The photocatalytic activity of SnO_2 and PS/SnO_2 nanofoams was evaluated by photodegradation of Rhodamine B (RhB). Photocatalytic tests varying RhB concentration were carried out at $1.0x10^{-4}$, $1.5x10^{-5}$ and $3.0x10^{-5}$M. Tests were also conducted to observe the influence of catalyst weight, being investigated the concentrations of 0.1, 0.4 and 0.8 g/L. To find an optimal pH for the photocatalytic activity, tests were made at pH 4.0, 7.0 and 8.0 using appropriate aliquots of 0.1 M NaOH solution, and 0.1 M HCl solution. After the addition of PS/SnO_2photocatalyst, the system was kept in the dark for 30 minutes at 25 ºC, to ensure adsorption/desorption equilibrium of RhB on the photocatalyst surface and then irradiated with 3 × Phillips 15 W lamps (45 W), emitting UV radiation λ = 254 nm. The lamps were set in a closed photocatalytic chamber of dimensions 60 cm (height) x 80 cm (width) x 90 cm (height). Aliquots were collected for spectrophotometric analysis every 10 minutes during 70 min under irradiation. Assays were performed in triplicate and samples were stored in test

tubes covered with aluminum foil to prevent light exposure, prior to spectrophotometric analysis in the UV-visible region using a Shimadzu UV-2550 spectrometer.

3. RESULTS AND DISCUSSION

3.1 PS foams

The foams made from PS solutions at an initial concentration of 1.0% showed no structure or strength, and resulted in fragile materials not suitable for this work. On the other hand, the foams obtained from PS concentrations of 2.5 and 5.0% were compact, and robust, so these were used to make PS/SnO_2 nanofoams (Figure 1).

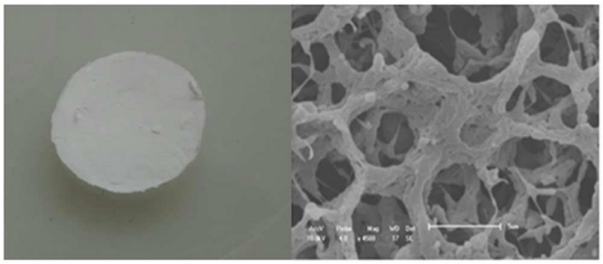

Figure 1. Left: Foam of PS (2.5), rigid and compact with average size of 3 cm. Right: PS foam SEM image showing porous structure (bar scale = 5 μm).

During freeze-drying, given the samples remain below the glass transition temperature of PS and melting point of CH, the solvent is removed to give porous structures, with voids resulting from the removal of the CH solvent. The temperature at which the dispersion in cyclohexane solvent is annealed for freezing is a primary factor in the preparation of foams. The mixture should be at or above the theta temperature at which mixtures from stable dispersions. At the theta temperature, the polymer chains behave as ideal chains, having no preferential interactions with solvent or between chain segments, behaving similarly to the melt state[18,24]. For temperatures below theta the systems separate into two phases, one polymer rich and another polymer poor, which

results in poor distribution of polymer in the porous structure of the final material[18,25–27]. The theta temperature for PS/CH solutions is 36 ºC[18] , and as described by Aubert and Clough, the porous foam structures form in such a way (below theta) that the mixtures would separate into two liquid phases, one PS-rich and other CH-rich. However, if these mixtures are very quickly quench-frozen at temperatures below the melting point of CH (+6 °C), nuclei of the liquid PS/CH-rich phase will become entrapped inside the frozen CH-rich phase. Once a frozen CH-rich phase is nucleated in the freeze-drying process, more CH migrates from the liquid PS-rich phase to the CH-rich phase, enriching further the polymer concentration. That means the porosity of the final material will be a function of the polymer concentration in the PS-rich domains. The final state of the system is a CH-free solid porous PS material with an open cell-like foam structure[18]. Another way of thinking about this freeze-drying process is that the frozen CH solvent acts as a porogen to produce porous materials[28].

3.2 SnO_2 nanoparticles and PS/SnO_2

Figure 2 shows the XRD patterns for PS(2.5)/SnO_2(5)-700 nanofoams and for the SnO_2-700 nanoparticles to highlight possible changes resulting from the incorporation of nanoparticles into the polymeric foams. Being an amorphous polymer polystyrene does not give rise to any significant XRD peaks[29]. X-ray diffraction from the PS(2.5)/SnO_2(5)-700 system proves tin oxide is incorporated in the nanofoam, and also shows changes related to the presence of polystyrene. Comparing before and after impregnation in PS foams, observation of the tetragonal phase (JCPDS - 88-0287) indicates SnO_2 in the nanofoams[30–32], which is observed for all samples. The band over the region between 10 and 19.42° indicates formation of a non-crystalline structure, which, according to Botan *et al.*[33], is characteristic of polystyrene, additionally there is small peak broadening for SnO_2, as shown in the *Full Width at Half Maximum* (FWHM)

values calculated from the XRD pattern. The amorphous polymer structure was maintained during the TIPS process, whereas the FWHM broadening for SnO_2 can be attributed to a better dispersion of the SnO_2 decreasing the agglomeration. This observation suggests possible changes in photocatalytic activity may be observed (see below), due to increased surface area.

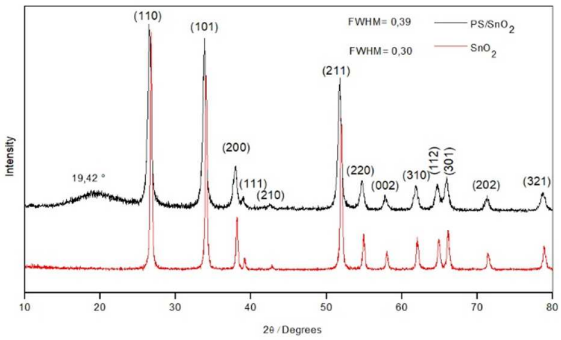

Figure 2. X-Ray diffractograms of PS(2.5)/SnO_2(5)-700 nanofoams compared to bare SnO_2-700.

The FWHM values were obtained using the PeakFit software and the crystallite sizes were calculated using the Scherrer equation[34], calculated using the most intense peak of in the XRD (110).The results are summarized in Table 1, showing that nanoparticles were obtained in all cases and their sizes increase as the initial samples are heated to higher temperatures.

Table 1: Structural and electronic parameters for SnO_2 and PS/SnO_2

SnO_2 (T °C)	**Crystallite Size (D_c, nm)**	**FWHM – SnO_2**	**$S_{B.E.T}$ (m^2/g) – SnO_2**	**Band gap (eV) – SnO_2**	**$S_{B.E.T}$ PS(2.5)/SnO_2(5)-700**
700	22.7	0.39	15.2	3.0	48.7

800	27.0	0.33	14.9	2.9	34.8
900	30.8	0.29	11.6	2.8	28.1

The results of the FWHM and crystallite size values were obtained from the XRD patterns and are presented in Table 1 (see also Fig. S2 in Supporting Information). It is observed that increasing temperature promotes crystallite growth and lowers FWHM values. This is consistent with temperature-induced crystallite nucleation occurring initially, and then growth with increasing temperature (due to high coalescence). As a consequence, the material is of higher crystallinity, according to the changes in FWHM values as a function of temperature, and smaller surface areas as indicated by the BET analyzes. According to Table 1, it is observed that increasing calcination temperature leads to lower surface area. The higher specific surface area at 700 °C may be attributed to more defects in SnO_2, which leads to tiny pores. At 900 °C these pores collapse, resulting in a smaller specific surface area[35]. Majumdar *et al.*[36] also conducted studies involving other synthetic methods for SnO_2, and concluded that heat treatment influences directly surface properties, just like as observed here. At high temperatures the studied oxides showed a significant decrease in surface area. It is suggested that calcination at 800º C and 900 ° C has led to further contraction of the porous structure, where some pores join to form larger voids resulting in reduction of surface area. These data corroborate the micrographs shown in TEM (see below), which indicate that one of the reasons for the change in surface area is the formation of aggregates/agglomerates with increasing calcination temperature, and the concurrent increase in particle size. Nonetheless, surface area values are still higher in the nanofoams than for the bare oxides. Studies conducted by Rumyantseva et al.[37] confirmed similar results to this study. They assessed the effect of heat treatment on the specific surface area and pore

volume for SnO_2 nanocrystalline powders and found that oxide calcined at lower temperatures resulted in greater surface area compared to higher temperature treatment.

The band gap energies for each sample were calculated using Tauc methodology[38]. The observed increase in absorbance with temperature is attributed narrowing of the SnO_2 band gap[28] owing to bigger particles sizes and surface roughness[39], leading to a higher absorbance for SnO_2-900 (Fig. S3 in Supporting Information).

Figure 3 shows HRTEM images for the SnO_2-700, 800 and 900. They show that the oxide powder contains nanoparticles with sizes varying roughly between 20 and 80 nm, depending on the heat treatment temperature. For agglomerated particles it was not possible to obtain accurate size measurements, however, the effect of temperature on particle size is clear[35].

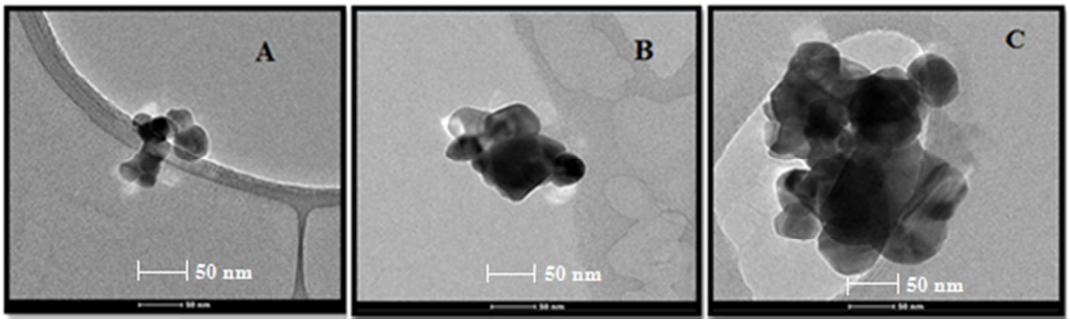

Figure 3. HRTEM images of the annealed SnO_2 nanoparticles at A) 700 B) 800, and C) 900 °C. (Size bar = 50 nm)

The same trends in nanoparticle size can be seen comparing these HRTEM results with crystallite sizes values obtained from X-Ray Diffraction.

3.3 Photocatalysis

3.3.1 Effects of polystyrene concentration

Initially, the influence of RhB concentration was investigated, and it was observed that low concentrations favored photocatalytic degradation (Fig. S4 in Supporting Information). Hu et al.[40] presented similar results for photocatalytic RhB degradation as

a function of concentration. Within 300 minutes, RhB degradation decreased from 94 to 70% when the initial RhB concentration increased from 10 to 25 mg. L^{-1}, consistent with an "inner filter-type" effect leading to a lower rate of photocatalytic degradation[40]. Tests were carried out to find the optimum PS level for RhB degradation, and Figure S4 shows photodegradation of RhB ($1.5x10^{-5}$mol/L) using PS(2.5)/SnO_2(2.5)-700 and PS(5)/SnO_2(2.5)-700 nanofoams.

According to Fig. S5 in Supporting Information the photocatalytic degradation of RhB in the presence of PS(2.5)/SnO_2(2.5)-700 appeared to be more effective compared to the PS(5)/SnO_2(2.5)-700 system. This could be owing to greater surface coverage of SnO_2 nanoparticles by PS at the higher level decreases accessibility to SnO_2 active sites, which in turn reduces photoactivity[41].

As shown in Figure 4, for a foam in the absence of SnO_2 nanoparticles there is only a maximum of 25% degradation after 70 min, showing that the presence of SnO_2 particles is needed for good photocatalytic performance. An increase in reaction rate leading to an almost complete RhB degradation (97.1%) in 70 minutes was observed with PS(2.5)/SnO_2(2.5)-700 nanofoam.

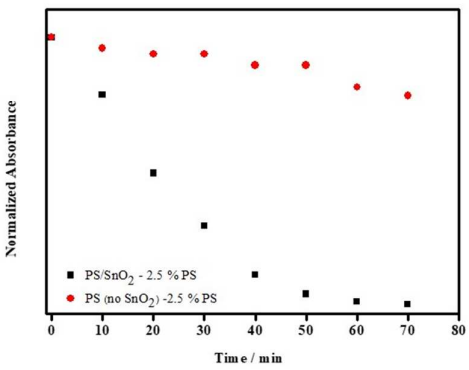

Figure 4. Photocatalytic degradation of RhB for PS(2.5)/SnO_2(2.5)-700 in comparison to only PS(2.5).

Thus, the presence and amount of SnO_2 greatly influence photocatalytic degradation. Regarding the mass concentration of photocatalyst Fig. S6 in Supporting Information shows that 0.4 g / L is the most appropriate of those tested. According to studies by Leea and Adesina[42], an increase in catalyst mass may cause light scattering and hence reduce the catalytic activity.

3.3.2 Photodegradation pathway

The photocatalytic degradation of RhB was studied as a model reaction to assess these photocatalytic nanofoams for applications in environmental remediation. Changes in the main UV-vis absorption spectra as a function of time and appropriate concentrations were followed to track evolution of the RhB degradation products shown in Supporting Information.

To confirm that the photocatalytic activity is due to the photocatalyst only, we carried out blank experiments without a catalyst under light (photolysis)[56], as shown in Fig. S7 in Supporting Information. It was observed that after 70 min, 20% of RhB was degraded. One explanation for this behaviour is that RhB dye can absorb UV radiation, and the energy is sufficient to break bonds in the chromophore groups. Photolysis, however, represents a small fraction of the photodegradation process and does not lead to effective and efficient degradation.

The spectral changes during the photocatalytic degradation of RhB under UV irradiation using SnO_2 particles are shown in Figure 5. As can be seen, the characteristic absorption band of RhB decreased rapidly, simultaneously with a hypsochromic shift in the absorption maximum from 554 to 534 nm. Previous studies have also reported similar changes using $NaBiO_3$ as photocatalyst[43]. The sharp decrease in the maximum absorption results from cleavage of the chromophore, whereas the peak displacement is

related to a N-de-ethylation mechanism: RhB is considered completely N-de-ethylated when displacement of the absorption maximum moves from 554 to 498 nm[44]. Thus, it was concluded that N-de-ethylation of RhB does occur in this case, however, it is not the predominant mechanism. It can be seen in Figure 5 that absorbance decreases more quickly than the maximum wavelength is shifted. This behavior clearly indicates that the chromophore cleavage mechanism predominates over N-de-ethylation when using SnO_2 as photocatalyst.

The effect of temperature treatment on catalyst performance for RhB degradation was evaluated (discussed below), and kinetic parameters for SnO_2-700, SnO_2-800 and SnO_2-900 samples are listed in Table 2. Catalysts treated at a lower temperature showed higher activity, and this can be understood as result of smaller nanoparticle size and subsequently larger surface area. Therefore, SnO_2-700 was selected to make PS/SnO_2 nanofoams for applications testing. It was noted that changing pH lead to no significant effect on dye degradation, although a small decrease in degradation efficiency at higher pH was noted (Fig. S8 in Supporting Information). Hence pH 4.0 was selected as the optimum condition for the reaction medium.

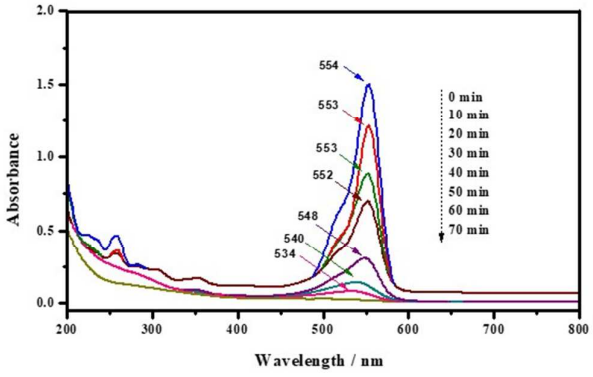

Figure 5. UV-vis absorption spectra of RhB degradation in the presence of bare SnO_2 as a function of time (catalyst dosage: 0.4 $g.L^{-1}$, C_{RhB}:1.0x10 $^{-5}$ mol/L, pH: 4.0)

The spectral changes during RhB photodegradation in the presence of PS/SnO_2 nanofoams are shown in Figure 6. The N-de-ethylation caused a shift in peak wavelength, resulting from the formation of a series of intermediate N-de-ethylation products of RhB, i.e., the ethyl groups were removed one by one, resulting in gradual changes in the peak maximum wavelength into the blue region[45]. The dye solution color disappeared (after 60 min irradiation), indicating that the chromophore was fully degraded. The generated products were identified as shown in Fig. S9 and S10 in Supporting Information, consistent with three N-de-ethylations. It can be observed that PS/SnO_2 nanofoams caused a higher N-deethylation in comparison with SnO_2-only suspensions.

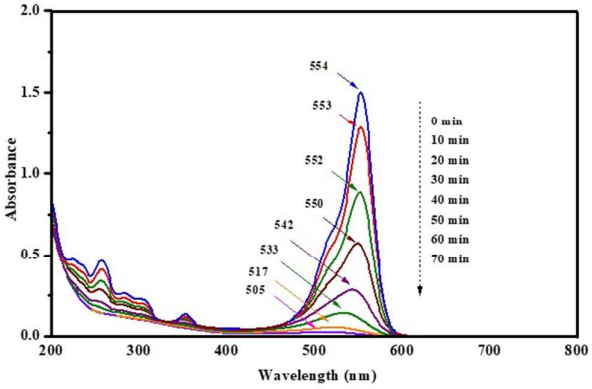

Figure 6. UV-vis absorption spectra of RhB up to 70 minutes in the presence of PS(2.5)/SnO_2(2.5)-700 nanofoams (catalyst dosage: 0.4 $g.L^{-1}$, C_{RhB}:1.0x10 $^{-5}$ mol/L, pH: 4.0).

Comparing the PS/SnO_2 and SnO_2 systems, the degradation mechanisms might differ, probably due to a stronger adsorption of RhB on the surface of PS/SnO_2 than on bare SnO_2, as discussed below. In general, these results showed that the PS(2.5)/SnO_2(2.5)-700 systems promote two competitive processes for the photodegradation of RhB, N-de-ethylation or cleavage of the chromophore. If both pathways occur simultaneously

this can enhance the rate of RhB degradation into colorless byproducts, and eventually to CO_2 and H_2O[46].

For SnO_2 only nanoparticle suspensions, the N-de-ethylation route was relatively less effective compared to cleavage, as noted. In contrast, when using PS/SnO_2 photocatalyst nanofoams, it was observed that, in addition to chromophore cleavage, a N-de-ethylation route opens up, consistent with the hypochromic shift to the blue region of the spectrum. Ortelli *et al*.[45] investigated degradation mechanisms of RhB, observing that the surface interactions semiconductor/dye dominate when the catalyst is well dispersed, leading to a degradation fully driven by OH• free radicals. In contrast, when the catalyst is supported or immobilized, substrate/dye interactions govern the N-de-ethylation process, driven by OH• radicals adsorbed on the surface.

3.3.3 Kinetics of RhB degradation

To better understand dye photodegradation the reaction kinetics were studied. Considering that the radiation source used has constant flux, and the number of photocatalyst active sites is solely dependent on the surface area, pseudo first-order kinetics are expected, provided there is no catalyst poisoning during the process.

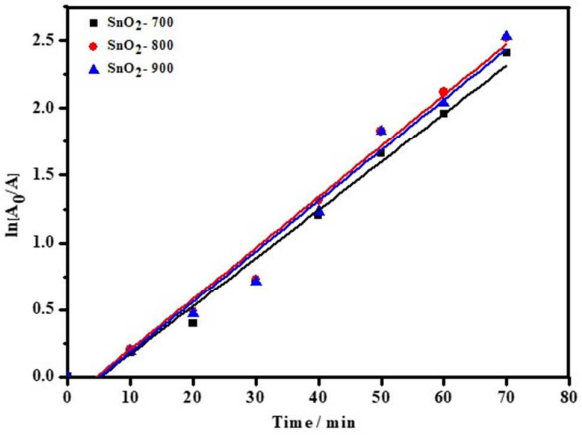

Figure 7. RhB photodegradation kinetics for SnO_2 treated at various temperatures (catalyst dosage: 0.4 $g.L^{-1}$, C_{RhB}:1.0x10 $^{-5}$ mol/L, pH: 4.59 (unadjusted))

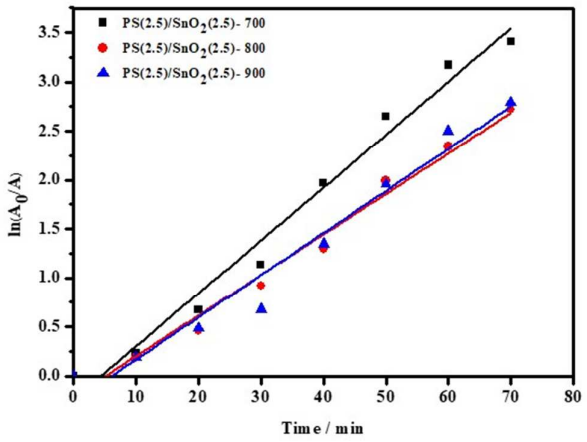

Figure 8. RhB photodegradation kinetics for PS/SnO_2 nanofoams at various SnO_2 temperature treatments (catalyst dosage: 0.4 $g.L^{-1}$, C_{RhB}:1.0x10 $^{-5}$ mol/L, pH: 4.60 (unadjusted))

Figure 7 and 8 show plots of $ln(A_0/A)$, s vs reaction time, for the system with bare SnO_2 and PS/SnO_2 nanofoams, respectively. A_0 is the RhB initial absorbance and A is the absorbance at the time t. (Assuming the Lambert-Beer law applies, absorbance is directly related to concentration.) Comparing all the nanofoams the PS(2.5)/SnO_2(2.5)-700 shows a higher photodegradation rate constant of 0.054 min^{-1}, as can be seen in Table 2, and this can be attributed to greater surface areas in nanoparticle-impregnated nanofoams SnO_2-700. Figures S11 and S12 in Supporting Information, show plots of A_0/A for degradation of RhB using SnO_2 only photocatalyst and SnO_2/PS foams, respectively. Comparison of the results obtained here with the available literature is not simple, since the process of photodegradation of dyes with UV and semiconductors depends on several factors, such as nature and concentration of the organic contaminant, concentration and type of semiconductor, light source, lamp power and intensity, pH, temperature, etc.[47]. In general, each piece of work employs different conditions,

however, given these limitations an appraisal of the performance of different system is made below.

Zhu et al.[48], studied the photocatalytic activity of SnO_2 microspheres for RhB degradation. They also observed pseudo-first order kinetics, and rate constants can be compared with those presented here. Zhu et al. analyzed different pH values, 2.91, 6.18 and 9.05, giving rate constants 0.0082, 0.0273 and 0.0195 min^{-1}, respectively. According to [48] these results may be associated with N-de-ethylation of RhB, since, as shown in Fig. 8, N-de-ethylation cannot be totally avoided and will occur in parallel with the direct degradation pathway. In addition, it should be noted that RhB photodegradation with two different catalysts (SnO_2 and PS/SnO_2) shows two changes: a rapid decrease in absorbance, and also a hypochromic shift of λ_{max}, which was confirmed by Watanabe[49] as being due to the N-de-ethylation of RhB, where the product is RhB (λ_{max} = 498 nm). In the present work, with two types of different catalysts (SnO_2 and PS/SnO_2), the blue shift was 15 and 44 nm at pH 4.0 consistent with the state of the catalyst dispersion affecting the photocatalytic degradation.

Table 2. Values of the degradation rate constants and the extent of degradation for all the systems studied under optimal experimental conditions. r^2 were all >0.97.

Photocatalyst	$S_{B.E.T}$ (m^2/g)	pH	k (min^{-1})	% (Photobleaching)
SnO_2-700	15.16	4.0	0.037	94.0
SnO_2-800	14.86	4.0	0.036	91.8
SnO_2-900	11.63	4.0	0.034	88.1
PS(2.5)/SnO_2(2.5)-700	48.69	4.0	0.054	98.2
PS(2.5)/SnO_2(2.5)-800	34.83	4.0	0.041	98.1
PS(2.5)/SnO_2(2.5)-900	28.12	4.0	0.043	96.1

Clearly, the degradation efficiency using nanofoams was significantly improved over the bare nanoparticles, since nanofoams provide higher surface area and porosity, and also allow easy recovery of the catalyst. This structure can affect the transport pathways, allowing dye molecules to reach active sites, meaning that porosity can improve the photocatalytic efficiency[50]. These results are comparable, and even better, than some reported ones, as shown in Table 3. Note that is not easy to compare these results, since besides RhB:SnO_2 molar ratio, irradiation power is an important factor, and the 60 W lamp used here is smaller than some others reported, such as 300 W for the work of Zhu et. al[48].

Table 3. Kinetic constants obtained here (best system) compared to other literature reports.

System	**RhB/SnO_2 (mol:mol)**	**k (min^{-1})**	**Irradiation**	**Ref.**
SnO_2- nanoporous (photochemical synthesis)	1:19	0.027	UV tube-like lamp. (254 nm, 8 W)	CHEN *et al.,* (2014)[51]
SnO_2- microspheres (solvothermal method)	1: 10	0.0273	high pressure mercury lamp (300 W)	ZHU *et al*., (2014)[48]
SnO_2 supported in mesoporous TiO_2 (sol–gel method)	1:15	0.010	UV lamp.	Abdel-Messih *et al* ., (2013)[52]
SnO_2/polystyrene (polymer precursors)	1: 88	0.054	UVC germicidal lamp.(254 nm, 60 W)	This work

3.3.4 Catalyst reuse

A large amount of disposable PS by-products cause serious environmental problems, this waste has been dubbed "white pollution". Polystyrene waste is not economically viable for recycling, but can be employed to remove other pollutants present in various environments such as water. If the produced material proves highly effective for degradation of pollutants, like dyes, it could have important industrial applications in water remediation systems. An attractive aspect of the work described here is the potential to reuse waste PS in environmental remediation applications[53]. To further investigate the reuse of PS(2.5)/SnO_2(2.5)-700 nanofoams, they were subjected to five successive use cycles for photodegradation of rhodamine B. Figure 9 shows the changes in catalyst effectiveness after five reuse cycles.

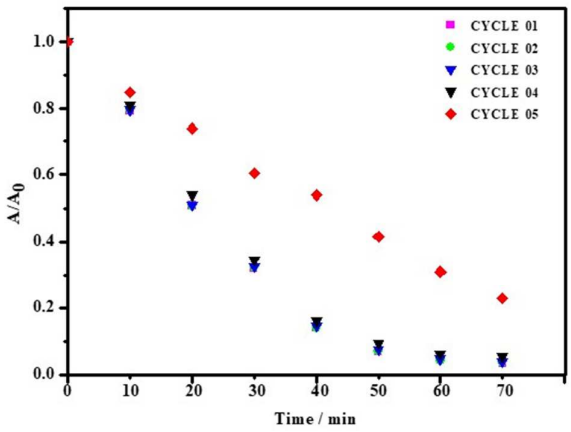

Figure 9. Reuse of a PS(2.5)/SnO_2(2.5)-700 nanofoam photocatalyst for RhB degradation.

The first run showed 98.3% of RhB degradation; cycle 2, 98.3%; cycle 3 showed 97.8% degradation; cycle 4, 96.5% and the fifth degraded 82% of the initial dye. Unfortunately, there was a decrease in nanofoam activity from the fifth reuse. These results indicate that nanofoams exhibit stable photocatalytic activity, which is a very important factor for practical applications[44], and also demonstrate the feasibility of

waste polystyrene reuse for environmental remediation of effluent dyes. It is possible that successive reuse and washing brings about a modification of the interfacial structure, altering its capacity for catalysis. An alternative reason is UV-induced photodegradation of the PS structure. Altin and Sokmen[53], also carried out study of reuse of catalysts based on polystyrene. The photocatalytic properties of the produced material were tested for degradation and removal of methylene blue (MB). It was noted the TiO_2-PS activity decreased nearly 50% for MB removal after 5 cycles, and the TiO_2-PS catalysts were still effective albeit with lower dye removal rates.

4. CONCLUSIONS

Polystyrene was successfully converted from waste commercial pellets into nanofoams using a thermally induced phase separation (TIPS) method. The incorporation of SnO_2 nanoparticles generated composite nanofoams, being novel photocatalysts which were assessed for potential environmental applications by following degradation of a model pollutant dye RhB. The functional nanofoams made from SnO_2 nanoparticles annealed at 700ºC resulted in higher photocatalytic activity in this application than if treated at a higher temperature of 900 ºC. This temperature effect was accounted for in terms of a decrease in effective nanofoam surface area after annealing at the higher temperature. Irradiating RhB solutions in the presence of PS/SnO_2 nanofoam photocatalysts resulted in a final degradation of 98.2%, which is better than reported in literature for SnO_2 nanoparticles[54]. This improved photocatalytic performance of the PS/SnO_2 nanofoams was attributed to larger surface areas and greater porosities compared to SnO_2 nanoparticles. The porous nanofoam structures favor interactions between dye molecules and OH radicals on the foam surfaces, leading to dye degradation, principally by N-de-ethylation[45]. As such, porous structures offer more catalytically active sites, and hence improved surface stability of electrons and holes to generate hydroxyl radicals, which may react to degrade contaminants. Additionally, the porous channel structure may facilitate better transport of contaminant molecules to reach catalytically active sites[55]. Reaction kinetics analyses reinforce that incorporation of the SnO_2 nanoparticles into the PS foams improves RhB photodegradation, with rate constants as high as 0.054 min^{-1}, being similar/higher than other reported systems, which are sometimes chemically more complex than these nanofoams[48,51,52]. Reuse of the PS/SnO_2 nanofoams was demonstrated over five photocatalytic cycles, showing retention of activity for up to 4 cycles, but loss of

efficiency only after the fifth cycle. This proof of principle work offers an interesting two-fold environmental advantage: firstly, the feasibility to reuse polymeric waste to fabricate new materials, which secondly, can be employed to tackle another environmental issue, water treatment. New possibilities are being studied, with incorporation of catalysts (gold, silver, gold/palladium) and adsorbents (dolomite) to evaluate new catalytic transformations and removal of pollutants from wastewater and underground water.

ASSOCIATED CONTENT

Supporting Information.

The Supporting Information is available free of charge on the ACS Publications website at DOI: 10.1021/acsami.xxxxxx.

X-ray diffractograms of SnO_2, crystallite size of SnO_2, Diffuse reflectance spectra of SnO_2, RhB photodegradation related to SnO_2 concentration, RhB photodegradation related to PS concentration, RhB photodegradation related to catalyst mass, RhB photodegradation related to pH, Relation between RhB maximum wavelength and absorbance with time for SnO_2 and PS/SnO_2, A/A_0 vs time plots of RhB photodegradation over SnO_2 and PS/SnO_2 catalysts.

AUTHOR INFORMATION

Corresponding Author

Rodrigo José de Oliveira

+55 83 99816 2342, rodrigo@cct.uepb.edu.br

Corresponding Author

Julian Eastoe

Phone +44-117-928-9180, Julian.Eastoe@bris.ac.uk

Present Address

[Δ] Instituto de Química e Biotecnologia, Universidade Federal de Alagoas, Brazil.

ORCID

Rodrigo José de Oliveira: 0000-0002-8753-2661

Julian Eastoe: 0000-0001-5706-8792

Author Contributions

All authors have given approval to the final version of the manuscript and contributed to the final version of the manuscript.

ACKNOWLEDGEMENTS

RJdeO acknowledges CAPES agency for financial support, University of Bristol UK for a Benjamin Meaker Research Fellowship, CETENE for transmission electron microscopy images, and IQ-UnB for surface area analysis and XRD analysis. GCdeA acknowledges CAPES agency for a student scholarship.

REFERENCES

(1) Chowdhury, S.; Balasubramanian, R. Graphene/semiconductor Nanocomposites (GSNs) for Heterogeneous Photocatalytic Decolorization of Wastewaters Contaminated with Synthetic Dyes: A Review. *Appl. Catal. B Environ.* **2014**,

160–161, 307–324.

(2) Srinivasan, A.; Viraraghavan, T. Decolorization of Dye Wastewaters by Biosorbents: A Review. *J. Environ. Manage.* **2010**, *91*, 1915–1929.

(3) Nagaraja, R.; Kottam, N.; Girija, C. R.; Nagabhushana, B. M. Photocatalytic Degradation of Rhodamine B Dye under UV/solar Light Using ZnO Nanopowder Synthesized by Solution Combustion Route. *Powder Technol.* **2012**, *215–216*, 91–97.

(4) Pascariu, P.; Airinei, A.; Olaru, N.; Olaru, L.; Nica, V. Photocatalytic Degradation of Rhodamine B Dye Using ZnO–SnO2 Electrospun Ceramic Nanofibers. *Ceram. Int.* **2016**, *42*, 6775–6781.

(5) Saharan, V. *Advanced Oxidation Technologies for Wastewater Treatment: An Overview*; 2015.

(6) Ben Ali, M.; Barka-Bouaifel, F.; Sieber, B.; Elhouichet, H.; Addad, A.; Boussekey, L.; Férid, M.; Boukherroub, R. Preparation and Characterization of Ni-Doped ZnO–SnO2 Nanocomposites: Application in Photocatalysis. *Superlattices Microstruct.* **2016**, *91*, 225–237.

(7) Glaze, W. H.; Kang, J.-W.; Chapin, D. H. The Chemistry of Water Treatment Processes Involving Ozone, Hydrogen Peroxide and Ultraviolet Radiation. *Ozone Sci. Eng.* **1987**, *9*, 335–352.

(8) Townsend, T. K.; Sabio, E. M.; Browning, N. D.; Osterloh, F. E. Photocatalytic Water Oxidation with Suspended Alpha-Fe2O3 Particles-Effects of Nanoscaling. *Energy Environ. Sci.* **2011**, *4*, 4270–4275.

(9) Gaya, U. I.; Abdullah, A. H. Heterogeneous Photocatalytic Degradation of Organic Contaminants over Titanium Dioxide: A Review of Fundamentals, Progress and Problems. *J. Photochem. Photobiol. C Photochem. Rev.* **2008**, *9*, 1–

12.

(10) Kohtani, S.; Makino, S.; Kudo, A.; Tokumura, K.; Ishigaki, Y.; Matsunaga, T.; Nikaido, O.; Hayakawa, K.; Nakagaki, R. Photocatalytic Degradation of 4-N-Nonylphenol under Irradiation from Solar Simulator: Comparison between BiVO 4 and TiO 2 Photocatalysts. *Chem. Lett.* **2002**, *31*, 660–661.

(11) Robinson, T.; McMullan, G.; Marchant, R.; Nigam, P. Remediation of Dyes in Textile Effluent: A Critical Review on Current Treatment Technologies with a Proposed Alternative. *Bioresour. Technol.* **2001**, *77*, 247–255.

(12) Yasmina, M.; Mourad, K.; Mohammed, S. H.; Khaoula, C. Treatment Heterogeneous Photocatalysis; Factors Influencing the Photocatalytic Degradation by TiO2. *Energy Procedia* **2014**, *50*, 559–566.

(13) Benhaoua, B.; Abbas, S.; Rahal, A.; Benhaoua, A.; Aida, M. S. Effect of Film Thickness on the Structural, Optical and Electrical Properties of SnO2: F Thin Films Prepared by Spray Ultrasonic for Solar Cells Applications. *Superlattices Microstruct.* **2015**, *83*, 78–88.

(14) Das, S.; Jayaraman, V. SnO2: A Comprehensive Review on Structures and Gas Sensors. *Prog. Mater. Sci.* **2014**, *66*, 112–255.

(15) Enesca, A.; Baneto, M.; Perniu, D.; Isac, L.; Bogatu, C.; Duta, A. Solar-Activated Tandem Thin Films Based on CuInS2, TiO2 and SnO2 in Optimized Wastewater Treatment Processes. *Appl. Catal. B Environ.* **2016**, *186*, 69–76.

(16) Navalon, S.; Dhakshinamoorthy, A.; Alvaro, M.; Garcia, H. Metal Nanoparticles Supported on Two-Dimensional Graphenes as Heterogeneous Catalysts. *Coord. Chem. Rev.* **2016**, *312*, 99–148.

(17) Plantard, G.; Goetz, V.; Correia, F.; Cambon, J. P. Importance of a Medium's Structure on Photocatalysis: Using TiO2□coated Foams. *Sol. Energy Mater. Sol.*

Cells **2011**, *95*, 2437–2442.

(18) Aubert, J. H.; Clough, R. L. Low-Density, Microcellular Polystyrene Foams. *Polymer (Guildf).* **1985**, *26*, 2047–2054.

(19) Steytler, D. C.; Robinson, B. H.; Eastoe, J.; Ibel, K.; Dore, J. C.; MacDonald, I. Effects of Solidification of the Oil Phase on the Structure of Colloidal Dispersions in Cyclohexane. *Langmuir* **1993**, *9*, 903–911.

(20) de Melo, D. S.; Santos, M. R. C.; Santos, I. M. G.; Soledade, L. E. B.; Bernardi, M. I. B.; Longo, E.; Souza, A. G. Thermal and Structural Investigation of SnO2/Sb2O3 Obtained by the Polymeric Precursor Method. *J. Therm. Anal. Calorim.* **2007**, *87*, 697–701.

(21) Pavia, F. C.; La Carrubba, V.; Piccarolo, S.; Brucato, V. Polymeric Scaffolds Prepared via Thermally Induced Phase Separation: Tuning of Structure and Morphology. *J. Biomed. Mater. Res. Part A* **2008**, *86A*, 459–466.

(22) Lu, X.; Wei, A.; Fan, Q.; Wang, L.; Chen, P.; Dong, X.; Huang, W. Macroporous Foam of Reduced Graphene Oxides Prepared by Lyophilization. *Mater. Res. Bull.* **2012**, *47*, 4335–4339.

(23) Nireesha, G. R.; Divya, L.; Sowmya, C.; Venkateshan, N.; Babu, M. N.; Lavakumar, V. Lyophilization/freeze Drying—an Review. *Int. J. Nov. trends Pharm. Sci.* **2013**, *3*, 87–98.

(24) Alger, M. *Polymer Science Dictionary*; Springer Netherlands: Dordrecht, 2017.

(25) He, Z.; Zhu, Z.; Li, J.; Zhou, J.; Wei, N. Characterization and Activity of Mesoporous Titanium Dioxide Beads with High Surface Areas and Controllable Pore Sizes. *J. Hazard. Mater.* **2011**, *190*, 133–139.

(26) Wu, H.; Ma, J.; Zhang, C.; He, H. Effect of TiO2 Calcination Temperature on the Photocatalytic Oxidation of Gaseous NH3. *J. Environ. Sci.* **2014**, *26*, 673–682.

(27) Muthuvinayagam, A.; Melikechi, N.; Dennis Christy, P.; Sagayaraj, P. Investigation on Mild Condition Preparation and Quantum Confinement Effects in Semiconductor Nanocrystals of SnO2. *Phys. B Condens. Matter* **2010**, *405*, 1067–1070.

(28) Yu, J.; Wang, G.; Cheng, B.; Zhou, M. Effects of Hydrothermal Temperature and Time on the Photocatalytic Activity and Microstructures of Bimodal Mesoporous TiO2 Powders. *Appl. Catal. B Environ.* **2007**, *69*, 171–180.

(29) Moraes, S. B. de; Botan, R.; Lona, L. M. F. Synthesis and Characterization of Polystyrene/layered Hydroxide Salt Nanocomposites. *Quim. Nova* **2014**, *37*, 18–21.

(30) Salavati-Niasari, M.; Mir, N.; Davar, F. Synthesis, Characterization and Optical Properties of Tin Oxide Nanoclusters Prepared from a Novel Precursor via Thermal Decomposition Route. *Inorganica Chim. Acta* **2010**, *363*, 1719–1726.

(31) Wan, X.; Ma, R.; Tie, S.; Lan, S. Effects of Calcination Temperatures and Additives on the Photodegradation of Methylene Blue by Tin Dioxide Nanocrystals. *Mater. Sci. Semicond. Process.* **2014**, *27*, 748–757.

(32) Sankar, C.; Ponnuswamy, V.; Manickam, M.; Mariappan, R.; Suresh, R. Structural, Morphological, Optical and Gas Sensing Properties of Pure and Ru Doped SnO2 Thin Films by Nebulizer Spray Pyrolysis Technique. *Appl. Surf. Sci.* **2015**, *349*, 931–939.

(33) Botan, R.; Gonçalves, N. A.; Moraes, S. B. de; Lona, L. M. F.; Botan, R.; Gonçalves, N. A.; Moraes, S. B. de; Lona, L. M. F. Preparation and Evaluation of Polystyrene (PS) – Layered Double Hydroxide (LDH) ZnAl – Organofunctionalized with Laurate/palmitate Nanocomposites. *Polímeros* **2015**, *25*, 117–124.

(34) Malagù, C.; Carotta, M. C.; Giberti, A.; Guidi, V.; Martinelli, G.; Ponce, M. A.; Castro, M. S.; Aldao, C. M. Two Mechanisms of Conduction in Polycrystalline SnO2. *Sensors Actuators B Chem.* **2009**, *136*, 230–234.

(35) Hao, Y.; Jiaqiang, X. U. Preparation, Characterization and Photocatalytic Activity of Nanometer SnO2. *Int. J. Chem. Eng. Appl.* **2010**, *1*, 241.

(36) Majumdar, S. The Effects of Crystallite Size, Surface Area and Morphology on the Sensing Properties of Nanocrystalline SnO2 Based System. *Ceram. Int.* **2015**, *41*, 14350–14358.

(37) Rumyantseva, M. N.; Gaskov, A. M.; Rosman, N.; Pagnier, T.; Morante, J. R. Raman Surface Vibration Modes in Nanocrystalline SnO 2 : Correlation with Gas Sensor Performances. *Chem. Mater.* **2005**, *17*, 893–901.

(38) Wood, D. L.; Tauc, J. Weak Absorption Tails in Amorphous Semiconductors. *Phys. Rev. B* **1972**, *5*, 3144–3151.

(39) He, Z.; Zhu, Z.; Li, J.; Zhou, J.; Wei, N. Characterization and Activity of Mesoporous Titanium Dioxide Beads with High Surface Areas and Controllable Pore Sizes. *J. Hazard. Mater.* **2011**, *190*, 133–139.

(40) Hu, L.; Yuan, H.; Zou, L.; Chen, F.; Hu, X. Adsorption and Visible Light-Driven Photocatalytic Degradation of Rhodamine B in Aqueous Solutions by Ag@AgBr/SBA-15. *Appl. Surf. Sci.* **2015**, *355*, 706–715.

(41) Wang, C.; Shao, C.; Zhang, X.; Liu, Y. SnO2 Nanostructures-TiO2 Nanofibers Heterostructures: Controlled Fabrication and High Photocatalytic Properties. *Inorg. Chem.* **2009**, *48*, 7261–7268.

(42) Lea, J.; Adesina, A. A. The Photo-Oxidative Degradation of Sodium Dodecyl Sulphate in Aerated Aqueous TiO2 Suspension. *J. Photochem. Photobiol. A Chem.* **1998**, *118*, 111–122.

(43) Yu, K.; Yang, S.; He, H.; Sun, C.; Gu, C.; Ju, Y. Visible Light-Driven Photocatalytic Degradation of Rhodamine B over NaBiO 3 : Pathways and Mechanism. *J. Phys. Chem. A* **2009**, *113*, 10024–10032.

(44) Moraes, S. B. de; Botan, R.; Lona, L. M. F. Synthesis and Characterization of Polystyrene/layered Hydroxide Salt Nanocomposites. *Quim. Nova* **2014**, *37*, 18–21.

(45) Ortelli, S.; Blosi, M.; Albonetti, S.; Vaccari, A.; Dondi, M.; Costa, A. L. TiO2 Based Nano-Photocatalysis Immobilized on Cellulose Substrates. *J. Photochem. Photobiol. A Chem.* **2014**, *276*, 58–64.

(46) Chen, G.; Ushida, T.; Tateishi, T. Development of Biodegradable Porous Scaffolds for Tissue Engineering. *Mater. Sci. Eng. C* **2001**, *17*, 63–69.

(47) Byrappa, K.; Subramani, A. K.; Ananda, S.; Rai, K. M. L.; Dinesh, R.; Yoshimura, M. Photocatalytic Degradation of Rhodamine B Dye Using Hydrothermally Synthesized ZnO. *Bull. Mater. Sci.* **2006**, *29*, 433–438.

(48) Zhu, Z. F.; Zhou, J. Q.; Wang, X. F.; He, Z. L.; Liu, H. Effect of pH on Photocatalytic Activity of SnO2 Microspheres via Microwave Solvothermal Route. *Mater. Res. Innov.* **2014**, *18*, 8–13.

(49) Watanabe, T.; Takizawa, T.; Honda, K. Photocatalysis through Excitation of Adsorbates. 1. Highly Efficient N-Deethylation of Rhodamine B Adsorbed to Cadmium Sulfide. *J. Phys. Chem.* **1977**, *81*, 1845–1851.

(50) Zhu, C.; Lu, B.; Su, Q.; Xie, E.; Lan, W. A Simple Method for the Preparation of Hollow ZnO Nanospheres for Use as a High Performance Photocatalyst. *Nanoscale* **2012**, *4*, 3060–3064.

(51) Chen, W.; Sun, F.; Zhu, Z.; Min, Z.; Li, W. Nanoporous SnO2 Prepared by a Photochemical Strategy: Controlling of Specific Surface Area and Photocatalytic

Activity in Degradation of Dye Pollutants. *Microporous Mesoporous Mater.* **2014**, *186*, 65–72.

(52) Abdel-Messih, M. F.; Ahmed, M. A.; El-Sayed, A. S. Photocatalytic Decolorization of Rhodamine B Dye Using Novel Mesoporous SnO2–TiO2 Nano Mixed Oxides Prepared by Sol–gel Method. *J. Photochem. Photobiol. A Chem.* **2013**, *260*, 1–8.

(53) Altın, İ.; Sökmen, M. Preparation of TiO2-Polystyrene Photocatalyst from Waste Material and Its Usability for Removal of Various Pollutants. *Appl. Catal. B Environ.* **2014**, *144*, 694–701.

(54) Ji, X.; Bai, C.; Zhao, Q.; Wang, A. Facile Synthesis of Porous SnO2 Quasi-Nanospheres for Photocatalytic Degradation of Rhodamine B. *Mater. Lett.* **2017**, *189*, 58–61.

(55) Chen, H.; Zhang, D.; Zhou, X.; Zhu, J.; Chen, X.; Zeng, X. Controllable Construction of Ordered Porous SnO2 Nanostructures and Their Application in Photocatalysis. *Mater. Lett.* **2014**, *116*, 127–130.

Table of Contents Graphic